Electronic Journal of Structural Engineering

Original Article

Cite this: DOI:10.56748/ejse.24549

Received Date:13 November 2023
Accepted Date: 24 May 2024

1443-9255
https://ejsei.com/ejse
Copyright: © The Author(s). Published by Electronic Journals for Science and Engineering International (EJSEI). This is an open access article under the CC BY license. https://creativecommons.org/licenses/by/4.0/

Numerical Simulation of Steel Reinforced Lightweight Aggregate Concrete Beams Based on Analysis of Push-out Test

Jianwen Zhang*, Fanyu Zhao, Zhipeng XV
College of Civil Engineering, Henan University of Engineering, Zhengzhou, China
*Corresponding author: 511017988@qq.com

Abstract

To study the influence of bond-slip on the numerical simulation of steel reinforced lightweight concrete (SRLC) members, the push-out test and finite element analysis are carried out first, and then the nonlinear finite element simulation of SRLC beams is conducted. The calculated results are compared with the experimental results. Four factors as the concrete protective cover thickness, stirrup ratio, concrete strength and anchorage length of section steel are considered in the test. The constitutive relation of interface bonding slip be-tween the section steel and light concrete is introduced in the finite element analysis based on the test results. Finite element analysis of push-out specimen's results indicate that the normal stress of the section steel is the same on the same cross section and the stress gradient gradually decreases from the loading end to the free end. Specimens with equivalent restraint coefficient γ_e less than 0.01 will be subjected to split failure and those specimens with the coefficient γ_e greater than or equal to 0.01 will be subjected to push-off failure. The bearing capacity and slip value obtained by finite element computation is consistent with experiment results. The stress distribution, crack shape and load-deflection curve are analyzed in numerical simulation of SRLC beams. Influence factors involving shear span ratio and position of section steel are considered. Analysis results show that the mechanical properties of the SRLC beams are like that of the steel reinforced normal concrete (SRNC)beams. Diagonal shear failure is gradually transformed into flexural failure with the shear span ratio increasing. The load- deflection curve is obviously divided into three stages. Finite analysis results considering the slip between section steel and concrete agree well with the test results, while the capacity and stiffness without considering the slip are bigger than the experimental values.

Keywords

Section Steel, Lightweight Aggregate Concrete, Push-out Test, Numerical Simulation, Beam

1. Introduction

The bond-slip property is an important working performance of concrete structures, which affects the bearing capacity and deformation properties of structures and components. With the development of high-rise and large-span structures, steel reinforced concrete (SRC) structures are more and more widely used in buildings. Lightweight aggregate concrete (LAC) has the advantages of light weight, high strength, heat preservation, fire resistance and earthquake resistance. The use of SRLC structure in modern buildings shows its superiority (NATALLI and XAVIER et al, 2021; PECCE and CERONI et al, 2015). High-rise buildings have been built by LAC in the United States, Japan, and Europe for more than half a century. China has successfully used LAC to construct high-rise residential buildings and long-span bridges in Tianjin, Shanghai, and other places. The bond-slip performance between LAC and steel bars has been studied by Chen Y S (CHEN and ZENG et al, 2005), whose study shows that the bond stress distribution of LAC is more uniform than that of ordinary concrete. A conclusion that the bond performance between ceramite concrete and steel is not worse than that of ordinary concrete is proposed by Lu C Y (LU and WANG, 2007). The bond - slip relationship between recycled concrete and steel bars is like that of ordinary concrete which has a great relationship with the shape of steel bars (XIAO and LI et al, 2006). David (MITCHELL and MARZOUK, 2007) studies the bond performance of 80MPa high-strength lightweight concrete (HSLC) and offers some conclusions that the bond strength of HSLC is slightly larger than that of high-strength normal weight concrete (HSNC), and the bond stress slip curve shows very steep rising and falling sections. All these achievements actively promote the application of the new SRLC structure in civil engineering. Tianjin University, Shenyang Institute of Civil Engineering and Architecture, Suzhou University of Science and Technology and other research institutions have carried out experimental research and published relevant papers on SRLC beams, columns, and joints, but the research results do not reflect the influence of bond slip on the mechanical properties of the components (TIAN, 2007; WANG and LI et al, 2000; SHAO and MAO, 2005). With the development of computer technology, it is possible to use finite element methods to calculate new complex concrete structures. The problem of bond slip is the key point in finite element analysis (ZENG and XV et al, 2010; ASHRAF, 2006), so it is necessary to establish a reasonable bond element and determine a reasonable bond stiffness in SRLC structures and members. The establishment of the correct mathematical model of bond-slip and related parameters can accurately calculate and analyze the strength, stiffness, deformation, and crack development of the structural members of SRLC, and pro-vide technical support for promoting the research and application of the new structure. In a word, the bond-slip of SRLC is a basic problem in structures which needs to be further studied.

2. Push-Out Test

9 specimens are designed by orthogonal test method as shown in Table 1, where b and h are the section width and height of the specimen, f_{cu} is the compressive strength of the concrete cube, la is the anchoring length, and C is the thickness of the protective layer. The bonding properties of the section steel and lightweight concrete are studied by push-out test. The test device is shown in Figure 1. The strain of section steel flange and web, the strain of concrete surface, the slips of loading end and free end, and the cracks are measured in the test. The cross-section diagram of strain gauge arrangement is shown in Figure 2.

Table 1. Specimen specification

NO.	b / mm	h / mm	f_{cu} / MPa	l_a / mm	C / mm	Stirrup
L1	200	200	24.2	200	50	ϕ8@100
L2	250	250	24.2	400	75.5	ϕ8@200
L3	300	300	24.2	800	100	0
L4	250	250	25.3	200	75.5	0
L5	300	300	25.3	400	100	ϕ8@100
L6	200	200	25.3	800	50	ϕ8@200
L7	300	300	30.0	200	100	ϕ8@200
L8	200	200	30.0	400	50	0
L9	250	250	30.0	800	75.5	ϕ8@100

Strain gauges are arranged in the inside and outside of the flange and the web of the section steel. The distance between the section steel strain gauges is 50mm within 200mm from the loading end, and the distance between the strain gauges beyond 200mm is 100mm. The concrete strain gauges are pasted on the position corresponding to the steel flange and web strain gauges respectively, and the spacing is 100mm. Two dial indicators are arranged at the loading end and the free end respectively to

measure slip. The test was carried out on a 100-ton pressure test machine and loaded by displacement control. Each specimen is preloaded before formal loading to ensure the smooth running of the test.

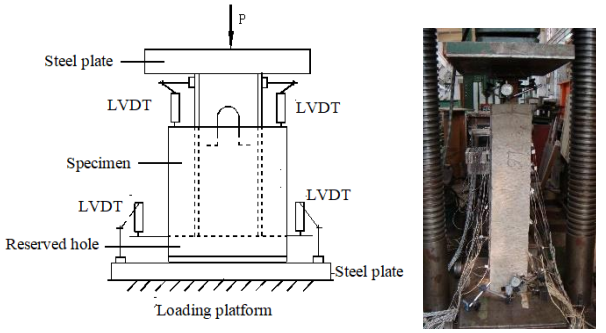

(a) Device drawing (b) Test photograph

Fig. 1 Test device picture

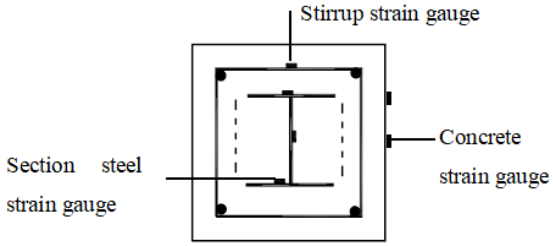

Fig. 2 Strain gauge layout profile

3. Ansys Simulate

The finite element analysis method is used to analyze different types of composed structures (ZHANG and MA, 2019; LI and YUAN et al, 2022; HAN and LIANG et al, 2023) in which valuable analysis results are obtained. The finite element simulation of SRLC push-out specimen is carried out as follows based on the reference of relevant literature. The analysis results are compared with the experimental results to provide reference for the analysis of SRLC members.

3.1 Element selection

1. Concrete unit. Concrete units are made of solid65. In this analysis the stirrup and longitudinal reinforcement are distributed in the concrete unit, and the effect of reinforcement on the unit is reflected by three different constants.
2. Section steel unit. The section steel and support plate are made of solid45 units. The unit is an 8-node hexahedral element, each node has 3 degrees of translation freedom UX, UY, UZ, which can be used for large deformation, large strain, and plasticity analysis.
3. Bonding unit. Combine39 unit is used as bonding unit. The longitudinal tangential bond slip F (bond force)-D(displacement) curve can be calculated by the measured bond constitutive relation. The normal deformation is much smaller than the longitudinal tangential deformation in the bonding failure problem, so it can be set as consolidation in this direction. There is no experimental data of the transverse tangential bond-slip, which is consolidated either considering the strong constraint effect of the stirrup on the flange and the flange restrain on the web.

3.2 Determination of real constants

Concrete constant

The real constant of solid 65 unit is R1, which contains parameters of the volume stirrup ratio in x, y and z directions and the direction angle of the bars.

Real constant of spring unit

The expressions of longitudinal tangential bond force F and displacement D can be determined by the bond slip curve. The relationship between the bonding stress τ and slip s at the corresponding position spring is determined as follows.

$$\tau = \tau(s, x_i) \quad (1)$$

The expression of F-D is:

$$F = \tau(D, x_i) \times A_i \quad (2)$$

Where A_i is the area of the corresponding node of the spring; x_i is the position coordinate of the spring.

The experimental results show that the bond stress at the loading end of the specimen has experienced a complete development process from rising to falling, which can be used as the basis for the local bond stress slip relationship. The bond-slip constitutive relationship obtained from the analysis of experimental data is expressed as follows (ZHANG, 2012):

$$\tau = (0.39445 + 2.5968s - 3.21651s^2 + 0.9678s^3)\tau_{f,\max} \quad (0 \le s \le 1.6\text{mm}) \quad (3)$$

Where $\tau_{f,max}$ is the maximum local bonding stress on the flange.

$$\tau_{f,\max} = 0.80839 + 0.07108 f_{cu} + 1.05327 \frac{c}{d} + 2.07355 \rho_{sv} \quad (4)$$

Where f_{cu} is the compressive strength of concrete; c is the thickness of the concrete protective layer; d is the height of section steel; ρ_{sv} is the stirrup ratio. The maximum value of local bond stress is not only related to the strength of concrete, but also to the stirrup ratio and the thickness of protective layer.

Liu Can (LIU and HE, 2002) believes that the bonding stress at the outer surface of the flange is 1.5 times that of the web. Zhang Yu's research on the section steel high-strength concrete shows that the bonding stress of the flange is twice that of the web (ZHANG and LI et al, 1999). The experimental results show that the maximum local bonding stress of the flange $\tau_{f,max}$ is 1.5 times that of the web, and the contribution of the web to the bonding stress cannot be ignored. When determining the real constant of the spring element it is necessary to consider both the dependent area of the element and the position whether the element is on the flange or on the web. The real constant of the spring element is shown in Figure 3.

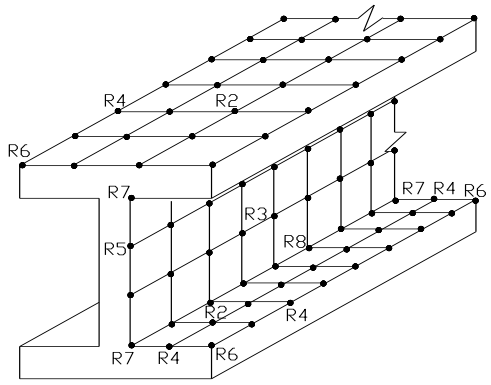

Fig. 3 Schematic diagram of real constant of spring element

3.3 Material constitutive relationship

Constitutive relationship of concrete material

The constitutive relation of lightweight aggregate concrete is the basis of finite element analysis. The constitutive model of concrete adopts the dynamic hardening model. The stress-strain curve including the ascending and descending sections can be expressed by a piecewise equation (ZHANG and CAO, 2008).

$$X \le 1, \quad Y = 1.5X - 0.5X^2 \quad (5)$$

$$X \ge 1, \quad Y = \frac{AX}{1 + BX + CX^2} \quad (6)$$

Where, $X = \frac{\varepsilon}{\varepsilon_0}$, $Y = \frac{f}{f_0}$ f_0 is peak stress, $\varepsilon_0$is peak strain. The study of stress-strain (f-ε) constitutive relation of light aggregate concrete shows that the peak strain, inflection point strain, inflection point stress, convergence point stress, convergence point strain all have linear relationship with the peak stress (WANG and SHAH, 1978). The three constants A, B, and C can be solved according to the three conditions satisfied by equations (5) and (6). The three conditions are the peak point stress is continuous, the peak point derivative is zero, and the stress and strain value at the convergence point satisfy equation (6).

Constitutive relationship for section steel and reinforcement

Bilinear isotropic hardening elastoplastic mode is adopted in the constitutive relationship model for section steel and reinforcement as shown in Figure 4, where f_y is the yield strength of the material, fu is the ultimate strength, and the Poisson ratio of the material is 0.3.

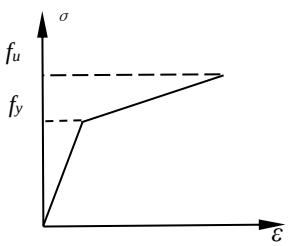

Fig. 4 Constitutive relation of section steel and bar

3.4 Finite element model establishment

After determining the element type, material properties and the real constant corresponding to the nonlinear spring element of concrete and section steel, the finite element analysis model of ANSYS program can be established. The following steps can be taken to build a model.

1. Select the required unit types and set the corresponding options and key parameters of each unit type.
2. Determine the material properties corresponding to each material and input the parameters into the corresponding tables.
3. Input the real constant corresponding to the nonlinear spring unit and check it in detail.
4. The finite element model is established by bottom-up approach in which the grid is divided into regular division. The 1/4 model is used for calculation.
5. According to the joint points divided by the section steel and concrete elements, the nonlinear spring element is generated.

To establish the spring element of the interface between section steel and concrete, we must first find out the corresponding rule of the joint, and then the spring element is set up by a cyclic statement, meanwhile its constant is assigned either.

The finite element model of specimen L1 is shown in Figure 5.

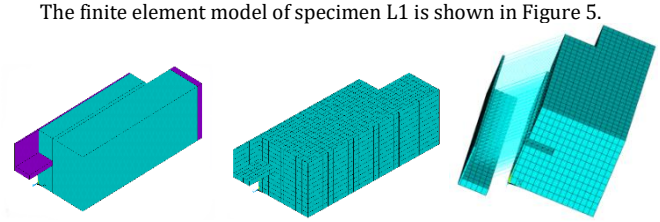

(a) Geometric model (b) Grid model (c) Spring unit model

Fig. 5 Finite element model diagram

Apply displacement constraint and displacement load to the established model, set calculation parameters and steps, and start the calculation.

4. Calculation Results and Analysis

4.1 Stress distribution of section steel

The cloud diagram of normal stress distribution of the section steel of specimen L3 under extreme load is shown in Figure 6 where the local bonding slip constitutive relation is introduced in finite element analysis.

As shown in Figure 6 the stress of the section steel is almost evenly distributed along the transverse plane at the same anchoring depth, which provides support for further theoretical analysis of the SRLC members. The stress value on flange and web are close to each other and can be considered equal in calculation and analysis. The cloud map also shows that the stress changes suddenly near the loading end, while the change slows down near the free end. This indicates that the bonding stress near the loading end is large, and the bonding stress gradually decreases from the loading end to the free end. The effect of binding force transferred to the concrete near the free end becomes less and less at the limit load. Therefore, the anchoring length should have a reasonable range.

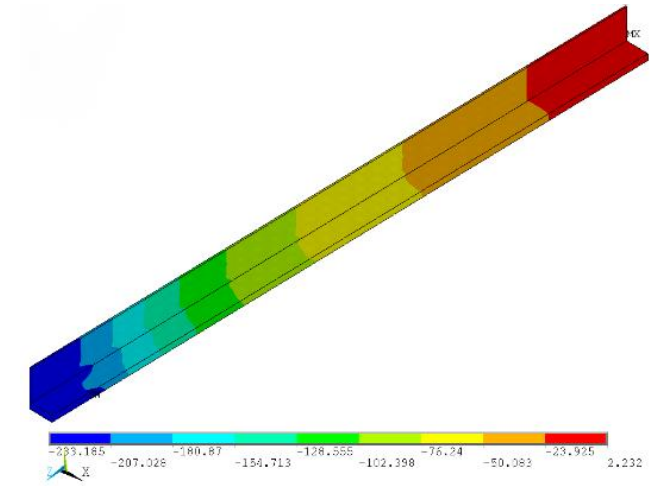

Fig. 6 Normal stress distribution nephogram of section steel

4.2 Crack Distribution

Figure 7 shows the crack distribution of specimens L8 and L9 under extreme load. Figure (a) is the fracture diagram of finite element calculation, and Figure (b) is the fracture diagram of test results.

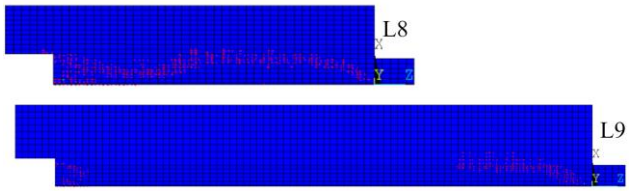

(a) Crack of finite element

(b) Experimental crack distribution

Fig. 7 Crack distribution

The crack distribution diagram shows that when the anchoring length is short, the thickness of the concrete protective layer is thin or the stirrup ratio is small, the splitting fracture failure occurs. When the ultimate load is reached, a long crack appears, such as specimen L8. When the anchoring length is longer, the thickness of the concrete protective layer is thicker or the stirrup ratio is more, the push-out failure of the specimen will occur. At the ultimate load, the load remains the same, while the slip continues to increase and tends not to converge. There are obvious cracks near the loading end, no cracks in the column body, and no obvious cracks in the free end, such as specimen L9. The specimens L1, L2, L3, L4, L7 and L8 were fractured and broken, and the other specimens were pushed out and failure. The finite element simulation results are consistent with the experimental results.

The test and calculation results show that the strength of the concrete restraint has an important influence on the failure form. Therefore, the equivalent constraint coefficient re is introduced to distinguish the failure type.

$$r_e = \rho_{sv} l_a C_1 / d^2 \tag{7}$$

Where ρ_{sv} is the stirrup ratio; la is the anchoring length; C is the thickness of section steel protective layer; d is the height of section steel.

Table 2 shows the equivalent constraint coefficients of specimens L1~L9. S stands for splitting failure, P for push-out failure. All specimens with equivalent constraint coefficient greater than or equal to 1.0 have push-out failure.

Table 2. Equivalent restraint coefficient r_e

Specimen	L1	L2	L3	L4	L5	L6	L7	L8	L9
γ_e（%）	0.5	0.6	0	0	1.34	1.0	0.34	0	2.48
Failure type	S	S	S	S	P	P	S	S	P

4.3 Load-slip curve

The comparison of the load-slip curves between calculated and test results of specimen L3 and L4 is shown in Figure 8. The peak point of the curve corresponds to the extreme load Pu and the extreme slip Su respectively. The comparison of calculated curves shows that the shape of calculated curves is consistent with that of test curves.

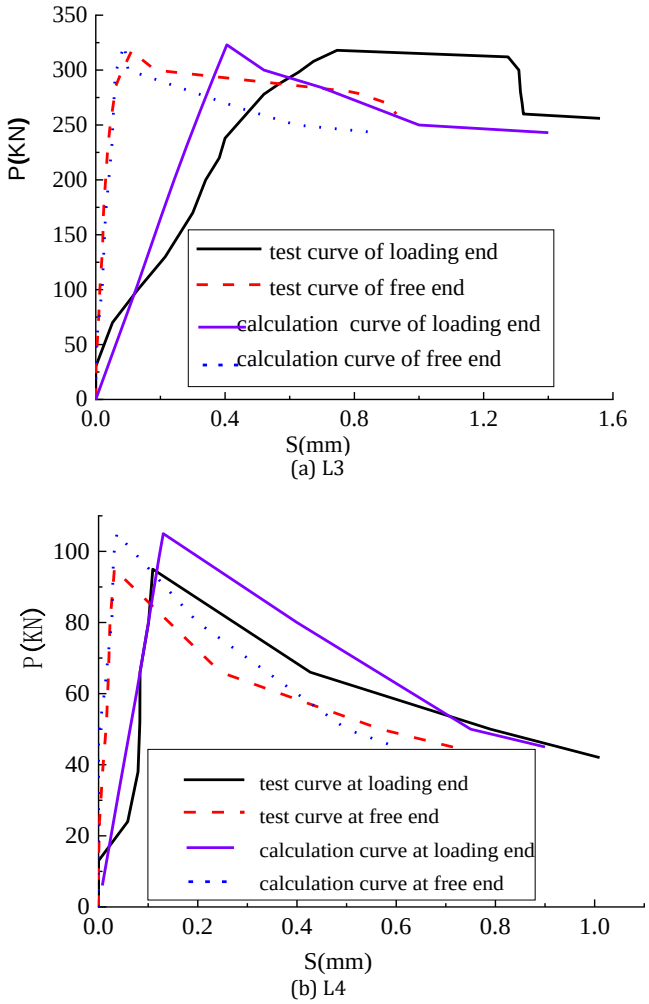

Fig. 8 Comparison of load slip curve

The calculated ultimate load is in good agreement with the experimental results, indicating that the local bonding stress-slip relationship can be used to simulate the ultimate load of the specimen.

The intersection point between the load-slip curve and the vertical axis is the initial slip load. The calculated initial slip load is smaller than the test value, and the average value of the ratio is 0.87. The main reason for this error is that the initial slip (0~ 0.1mm) section is simplified by linearization in the local bond-slip constitutive relationship. This simplification reduces the stiffness of the spring in the initial stage, resulting in a reduction of the initial slip load.

The ultimate load and the ultimate slip at the loading end are shown in Table 3, where Put and Sut are test values and P_{uc} and S_{uc} are calculated values.

Table 3. Comparison of calculated and test values

NO.	P_{ut} (KN)	S_{ut} (mm)	P_{uc} (KN)	S_{uc} (mm)	P_{uc} / P_{ut}	S_{uc}/ S_{ut}
L1	250	0.18	198	0.2238	0.792	1.243
L2	400	0.975	379	0.7691	0.948	0.789
L3	318	0.746	323	0.4056	1.016	0.544
L4	95	0.11	105	0.1305	1.105	1.186
L5	447	3.685	349	3.283	0.781	0.891
L6	361	8.783	368	8.954	1.019	1.019
L7	160	0.1795	171	0.1985	1.069	1.106
L8	307	0.45	305	0.394	0.993	0.876
L9	372	7.63	382	5.142	1.027	0.674

In Table 3 the average value of the ratio between the calculated limit load and the test value is 0.972, and the average value of the ratio between the calculated slip value and the test value is 0.925. Therefore, the mechanical properties of SRLC member can be well simulated by using the above method introduced in the bond-slip constitutive relationship.

5. SRLC Beam Numerical Simulation

5.1 Numerical simulation specimen

Numerical simulation specimens L1-L3 are selected from references (ZHANG, 2005; SHAO and MAO, 2005; WANG and WANG, 2005) respectively. The parameters of the specimens are shown in Table 4, and the section and calculation diagram are shown in Figure 9 and Figure 10 respectively.

Table 4. Specimen parameter

NO.	b×h (mm×mm)	a (mm)	b (mm)	L (mm)	λ	Steel	fcu (MPa)	ρss (%)
L1	200×300	275	200	2400	1.0	I12	26.6	3.017
L2	200×260	900	150	2500	3.83	I16	28.5	5.02
L3	170×270	565	100	2000	2.3	I10	25	3.12

Note: a is the distance from the concentrated load to the support; l is the beam length; λ is the shear span ratio; ρss is the section steel ratio.

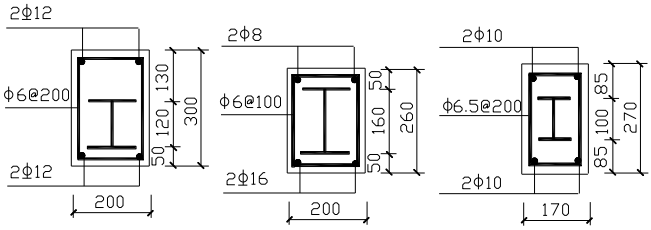

(a) L1 (b) L2 (c) L3

Fig. 9 Cross-section of the specimen

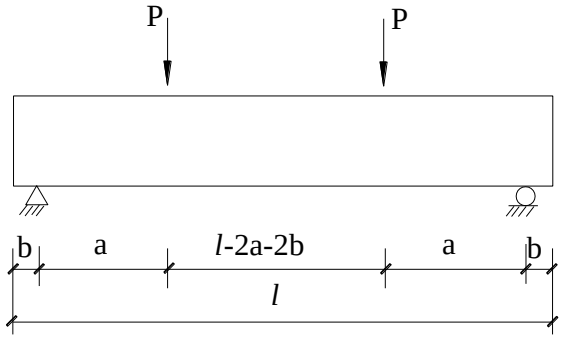

Fig. 10 Calculation diagram

5.2 ANSYS numerical simulation of SRLC beams

Finite element model establishment

The concrete unit adopts solid 65 and section steel unit adopts solid 45. The interface between section steel and concrete is coupled in normal and transverse direction, and the interface longitudinal connection unit adopts combine39. It can be seen from reference (ZHENG and LI et al, 2009) that the bond-slip curves of the tension zone and the compression zone of the section steel reinforced concrete beam are similar. Therefore, the constitutive relationship of the interface connecting element is the same in the tension zone and the compression zone. The concrete cracking shear transfer coefficient is 0.4, and closed shear transfer coefficient is 1.0. Concrete uniaxial tensile strength is input regardless of concrete crushing. The 1/2 model is adopted due to the symmetry of the structure.

Calculation results and analysis

1. Stress distribution cloud map of section steel

Figure 11 shows the stress distribution cloud diagram of the three specimens under ultimate load. The three specimens have different shear span ratio in which the section steel is arranged in two ways: symmetric and asymmetric. According to the stress distribution cloud diagram of section steel, the strain distribution of section steel under ultimate load meets the assumption of plane section. The shear span ratio λ of specimen L1 is 1 which occurs shear failure, and the tensile stress does not reach the yield strength under ultimate load. The shear span ratio of the specimens L2 and L3 is larger. Specimen L2 and L3 occur bending failure and bending shear failure respectively, in which the tensile stress of the section steel reaches the yield strength under ultimate load. The section steel of specimen L1 is placed in the tensile zone, and the maximum stress of the section steel in the tensile zone is only 109MPa when shear failure occurs which is less than half of its yield strength (235MPa). The section steel of specimen L2 is fully arranged in section. When bending failure occurs, the maximum stress in the tension zone of specimen L2 reaches the yield strength due to the rise of the neutral axis, while the maximum stress in the compression zone is 255MPa which does not reach the yield strength of 335MPa. The section steel of the specimen L3 is not fully arranged in

section. When bending shear failure occurs, the maximum stress in the tension zone reaches the yield strength with the rise of the neutral axis, while the maximum stress in the compression zone is only 82MPa which does not reach the yield strength.

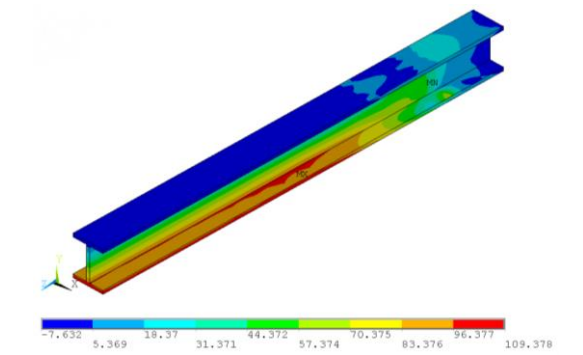

(a) L1

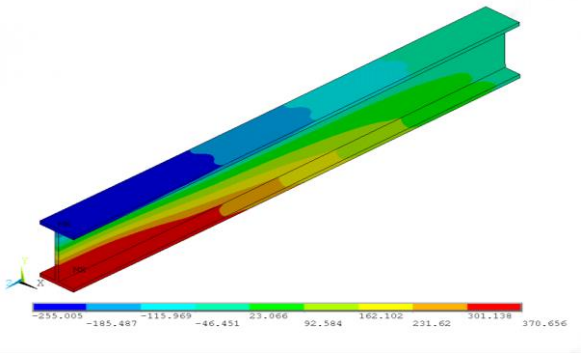

(b) L2

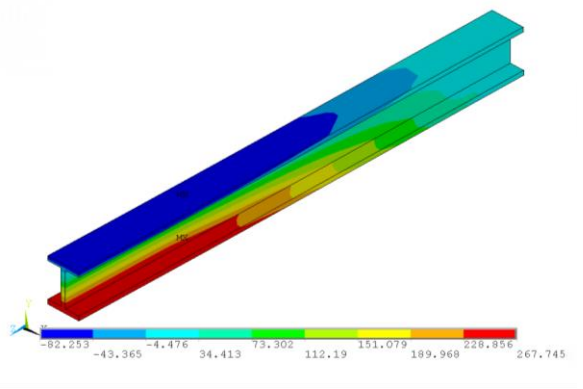

(c) L3

Fig. 11 Stress distribution diagram of section steel

2. Crack distribution pattern

Figure 12 shows the crack distribution of the three specimens under ultimate load.

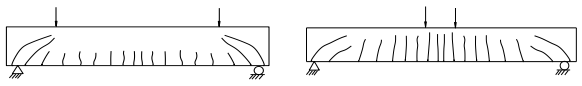

(a) L1 (b) L2

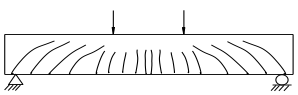

(c) L3

Fig. 12 Crack diagram

It can be seen from the crack distribution diagram that a main oblique crack forms from the loading point to the support under ultimate load for shear failure specimen L1, which is fully developed while the vertical crack in the bend section has not extended to half of the beam height. The bending failure occurred for specimen L2 in which the vertical crack height exceeds half of the section height. The bending shear failure occurred for specimen L3, in which both the vertical and oblique cracks are fully developed when failure happens.

3. Load-deflection curve

Specimen L2 suffered bending failure. Figure 13 shows the vertical displacement diagram under ultimate load. Figure 14 is a load-deflection curve graph in which the solid line represents the calculation curve, and the dashed line represents the test curve, and the two curves fit well. It can be seen from figure 13 that the P-F relationship curve can be divided into three distinct stages. The first stage OA is the elastic working stage; the second stage AB is the yield stage; the third stage BC is stiffness softening stage. Point B corresponds to ultimate bearing capacity and ultimate deformation.

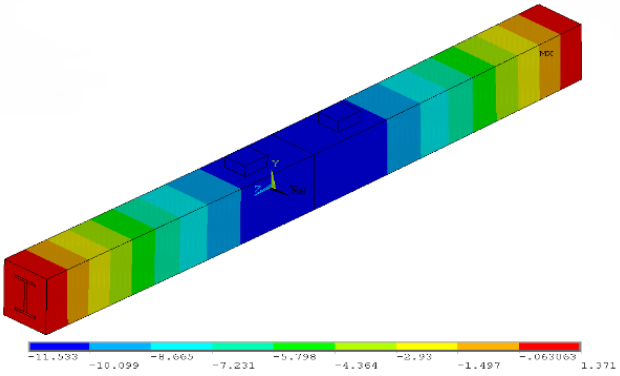

Fig. 13 Vertical displacement diagram of specimen L2

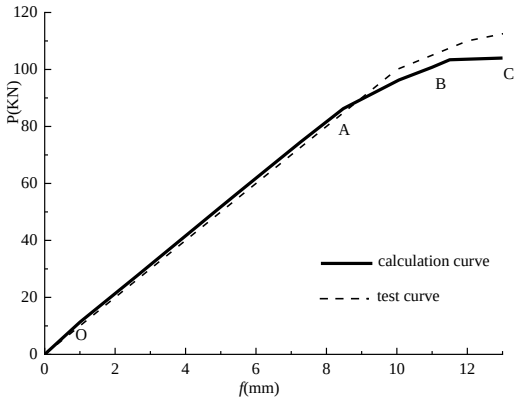

Fig. 14 Load-deflection curve of specimen L2

4. Comparison of bearing capacity

Shao Y J (SHAO and MAO, 2005) performed a finite element analysis of specimen L2 without considering bonding. The calculation results show that the calculated ultimate bearing capacity is 130KN which is 10.74% higher than the test value. The specimens L1 and L3 are calculated by the author using finite element method without considering bonding. The bearing capacity is 13.6% and 9.1% higher than the test value respectively. The stiffness of the specimens is greater than the true value due to the slip is not considered, so the calculated bearing capacity is higher than the test value.

The comparison of the finite element calculated value Puc and the test value Put of the specimens considering bond slip relationship is shown in Tab.5. The ratio between the calculated value and the test value is 98.7%. The calculated results of bearing capacity and deformation are in good agreement with the experimental results. It shows that the local bond-slip constitutive relationship can be well applied to the nonlinear finite element analysis of SRLC components.

Table 5. Comparison of bearing capacity

NO.	P_{uc}(KN)	P_{ut}(KN)	P_{uc} / P_{ut}
L1	115	110	1.05
L2	103.4	117.5	0.88
L3	80	78	1.03

6. Conclusions

Based on push-out test and finite element calculation, the finite element analysis of steel lightweight aggregate concrete beam is carried out. The finite element analysis results are in good agreement with the test results, and the main conclusions are as follows.

The bond stress reaches its maximum at the loading end and decreases with the increase of anchoring length. The bonding strength of the flange is calculated to be 1.5 times that of the web. According to the bond stress and slip at the loading end, the local bond slip constitutive

relation is established and the spring element is introduced into the finite element analysis.

With the increase of the equivalent constraint coefficient γe the failure mode of the specimen changes from splitting failure to push-out failure. The crack distribution and load-slip curves obtained by finite element analysis are in good agreement with the experimental results. The above analysis method can be applied to the finite element analysis for the SRLC members.

The finite element analysis of SRLC beam and SRC beam is carried out by the above method. The results show that the mechanical properties of SRLC beam and SRC beam are similar. When the shear span ratio is small, shear failure occurs which is gradually transformed to flexural shear failure and bending failure with the increase of shear span ratio. The load-deflection curve is divided into elastic section, yielding section and softening section. The calculated load capacity and stiffness of SRLC beam without considering bonding are larger than the experimental values, but the calculated results with considering bonding agree well with the experimental values.

Through the test and finite element research in this paper, there are still some limitations in the bond performance of section steel and lightweight aggregate concrete. For example, the bond slip performance of short-buried specimens and the constitutive relationship of light aggregate concrete need to be further studied. In this paper, the distribution law of bond stress of section steel and lightweight aggregate concrete with anchorage length of 200mm, 400mm and 800mm is studied. The local bond stress is obtained by the micro equilibrium equation. The determination of local bond strength depends on the strain data of the section steel and the calculation formula, which has a certain discretization. At present, there is more research on the constitutive relationship of normal concrete at home and abroad, but few on the constitutive relationship of light aggregate concrete. The constitutive relationship of materials is very important for accurate finite element analysis, so it is necessary to carry out in-depth research on the constitutive relationship of lightweight aggregate concrete to promote its application in practical engineering.

The minimum average bond strength in the test is 0.9MPa, which is not less than that of ordinary concrete. The minimum average bond strength of steel-shaped ordinary concrete in the references (Roeder, 1999) is 0.854MPa. The same calculation model can be used in the calculation of bearing capacity for both SRLC and SRC members. In view of its excellent seismic and load-bearing properties, it is necessary to vigorously develop the production and construction of light aggregate concrete, so that it can be more widely used in long-span and high-rise building projects.

References

Ashraf, A. 2006. Nonlinear analysis of reinforced concrete beam-columns with bond-slip. Journal of Engineering Mechanics, 132(11): 1177-1185. https://doi.org/10.1061/(ASCE)0733-9399(2006)132:11(1177)

Chen, Y. S., Zeng, S. H., Jiang, W. S. 2005. Experimental research on the bond stress distribution of deformed reinforcement in the lightweight reinforcement concrete. Journal of Hubei University of Technology, 20(2): 4-7. https://doi.org/10.3969/j.issn.1003-4684.2005.02.002

Han, T. C., Liang, S. T., Zhu, X. J., Wang, W. K., Yang, J. 2023. Numerical analysis of vertical behavior of large-span prestressed steel reinforced concrete slab. Journal of Southeast University, 53(2): 218-228. https://doi.org/10.3969/j.issn.1001-0505.2023.02.005

Li, Z., Yuan, X. L., Dong, T. F., Huang, Q., Deng, X. F. 2022. Anti-progressive collapse dynamic effect of RC beam-slab substructure under blast load. Journal of Vibration and Shock, 42(9): 27-46. https://doi.org/10.13465/j.cnki.jvs.

Liu, C., He, Y. B. 2002. Experimental study on bond behavior of steel reinforced concrete. Journal of Hunan University. 29(3):168-173. https://doi.org/1000-2472（2002）03-0168-06

Lu, C. Y., Wang, W. Y. 2007. Experiment research on bond behavior between deformed bar and lightweight concrete. Journal of Guangxi University, 32(1): 6-9. https://doi.org/10.3969/j.issn.1001-7445.2007.01.002

Mitchell, D. W., Marzouk, H. 2007. Bond characteristics of high-strength lightweight concrete. ACI Structural Journal, 104(1): 22-29.

Natalli, J. F., Xavier, E. M., Costa, L. C. B., Rodrigues, B. H., Sarmanho, A. M. C., Peixoto, R. A. F. 2021. New methodology to analyze the steel-concrete bond in CFST filled with lightweight and conventional concrete. Materials and Structures, 54(13). https://doi.org/10.1617/S11527-020-01579-5

Pecce, M., Ceroni, F., Bibbò, F. A., Acierno, S. 2015. Steel-concrete bond behavior of lightweight concrete with expanded polystyrene. Materials and Structures, 48: 139-152. https://doi.org/10.1617/s11527-013-0173-7

Roeder, C. W., Chmielowski, R., Brown, C, B. 1999. Shear connector requirements for embedded steel sections. Journal of Structural Engineering. 125, 142-151. https://doi.org/10.1061/(ASCE)0733-9445(1999)125:2(142)

Shao, Y. J., Mao, X. Y. 2005. Calculation method of bending strength of steel reinforced light aggregate concrete beam. Building Structure, 35(9):45-46. https://doi.org/10.19701/j.jzjg.2005.09.013

Tian, J. 2007. The computation of flexural rigidity of SRLC beam. Shanxi Architecture, 33(5): 5-6. https://doi.org/10.3969/j.issn.1009-6825.2007.05.003

Wang, L. G., Li, L. X., Li, J. X. 2000. Experimental research on the deformation of simply supported steel reinforced light aggregate concrete beams. Journal of Shenyang Architecture and Civil Engineering University, 16(3):179-181. https://doi.org/10.3321/j.issn:1671-2021.2000.03.006

Wang, L. G., Wang, C. 2005. Experimental study on the shear characteristic of steel encased light aggregate concrete beams. Industrial Construction, 35(1): 65-67. https://doi.org/10.3321/j.issn:1000-8993.2005.01.021

Wang, P. T., Shah, S. P., Naaman, A. E. 1978. Stress-strain curves of normal and lightweight concrete in compression. J.ACI, 75(11): 603-611. https://doi.org/10.1016/0148-9062(79)90235-3

Xiao, J. Z., Li, P. S., Qin, W. 2006. Study on Bond-slip between recycled concrete and rebars. Journal of Tongji University, 34(1):13-16. https://doi.org/10.3321/j.issn:0253-374X.2006.01.003

Zhang, J. J. 2005. The bearing capacity of the SRLC beam on the slanting section. Concrete. 2005(2): 39-42. https://doi.org/10.3969/j.issn.1002-3550.2005.02.010

Zhang, J. W. 2012. The bond stress-strain relationship for steel reinforced lightweight concrete. Mechanics in Engineering, 34(5): 52-56. https://doi.org/10.6052/1000-0879-12-229

Zhang, J. W., Cao, S. Y. 2008. Research on the stress-strain curves of structure lightweight aggregate concrete. Building Science, 24(11): 83-85.

Zhang, Y., Li, X. M., L, H. 1999. Bond behavior study of the steel reinforced high strength concrete structure. Building Structure. 29(7):3-5.

Zhang, Y. J., Ma, Q. G., Guo, J. W. 2019. Analysis of structural parameters of bridge with twin I-shaped steel beams and concrete slabs. Bridge Construction, 49(6): 66-71.

Zeng, L., Xv, C. X., Zheng, S. S., Lv, Y. 2010. Nonlinear finite element analysis on SRHSHPC frame joints. Earthquake Resistant Engineering and Retrofitting, 32(20): 37-41. https://doi.org/10.16226/j.issn.1002-8412.2010.02.008

Zheng, S. S., Li, L., Deng, G. Z. 2009. Experimental study on bond-slip behavior between shaped steel and HSHP concrete in steel reinforced HSHP concrete beams. Engineering Mechanics, 26(1): 104-111.